

## Electronic Supplementary Information (ESI)

### Accurate Synergy Effect of Ni-Sn Dual Active Sites Enhances Electrocatalytic Oxidation of Urea for Hydrogen Evolution in Alkaline Medium

Zhijiao Ji,<sup>a</sup> Jia Liu,<sup>\*a</sup> Yang Deng,<sup>a</sup> Shouting Zhang,<sup>a</sup> Zhen Zhang,<sup>a</sup> Peiyao Du,<sup>a</sup> Yanli Zhao,<sup>\*c</sup> Xiaoquan Lu<sup>\*ab</sup>

<sup>a</sup>Tianjin Key Laboratory of Molecular Optoelectronics, Department of Chemistry, School of Science, Tianjin University, Tianjin 300072, China.

<sup>b</sup>Department Key Laboratory of Bioelectrochemistry and Environmental Analysis of Gansu Province, College of Chemistry and Chemical Engineering, Northwest Normal University, Lanzhou 730070, China

<sup>c</sup>Division of Chemistry and Biological Chemistry, School of Physical and Mathematical Sciences, Nanyang Technological University, 21 Nanyang Link, Singapore 637371

Corresponding authors: luxq@tju.edu.cn, zhaoyanli@ntu.edu.sg, liujia@tju.edu.cn

#### EXPERIMENTAL SECTION

##### *Chemicals.*

All reagents were used without further purification. Isopropanol, nickel chloride hexahydrate ( $\text{NiCl}_2 \cdot 6\text{H}_2\text{O}$ ), thioacetamide (TAA) and tin tetrachloride ( $\text{SnCl}_4$ ) were purchased from Shanghai Aladdin Biochemical Technology Co. Ltd. Nafion 117 solution (5%) was purchased from Sigma-Aldrich. Potassium hydroxide (KOH) was purchased from Tianjin Damao Chemical. Milli-Q ultrapure water (resistance of  $18.2 \text{ M}\Omega \cdot \text{cm}^{-1}$  at  $25 \text{ }^\circ\text{C}$ ) was used for all experiments. Carbon paper was used as the substrate. Before preparing working electrode, the carbon paper was ultrasonic washed in ethanol and water two times each and dry in air.

### ***Synthesis of flower-like SnNiS precursor.***

Firstly,  $\text{NiCl}_2 \cdot 6\text{H}_2\text{O}$ ,  $\text{SnCl}_4$  and excess (TAA) were mixed in isopropanol (30 mL) to obtain uniform suspension, the molar ratios of  $\text{SnCl}_4$  to  $\text{NiCl}_2 \cdot 6\text{H}_2\text{O}$  were 1:0.3, 1:0.5, 1:0.7 and 1:1 respectively, and the fifth sample with the absence of  $\text{SnCl}_4$  was used as the control group. The suspension was transferred to a 50 mL *para*-polystyrene-lined (PPL) stainless steel autoclave and maintained at 180 °C for 24 h, and then allowed to cool down naturally. The obtained puce powder was washed with deionized water and ethanol several times and dried in the vacuum oven at 50 °C for 12 h. The SnNiS precursors were abbreviated as F-TNS (*i.e.*, F-TNS-0.3, F-TNS-0.5, F-TNS-0.7, and F-TNS-1), where the numbers of 0.3, 0.5, 0.7 and 1 represent the molar ratios of  $\text{NiCl}_2 \cdot 6\text{H}_2\text{O}$  to  $\text{SnCl}_4$  when preparing the precursors. The control group with the absent of  $\text{SnCl}_4$  was recorded as nickel sulfide (NS).

### ***Synthesis of particle-like NiSn sulfide.***

In order to obtain NiSn sulfide, the SnNiS precursor was stirred vigorously in 1 M KOH solution at 25 °C for three hours to dissolve  $\text{SnS}_2$ . Then, the product was washed with deionized water several times until the supernatant became neutral, which was dried in the vacuum oven at 50 °C for 12 h. Finally, the black NiSn sulfide electrocatalyst was synthesized. According to the SnNiS precursors used, the obtained catalysts were abbreviated as P-NTS-0.3, P-NTS-0.5, P-NTS-0.7, and P-NTS-1. The control group was recorded as NS-KOH, meaning that nickel sulfide (NS) was etched by 1M KOH.

### ***Catalyst characterization.***

The surface morphologies and compositions of the investigated materials were observed by field-emission scanning electron microscopy (FE-SEM) (Hitachi, SU8010). The transmission electron microscopy (TEM) characterization and electron diffraction analysis were conducted by JEM-JEOL2100F. Atomic force microscopy (AFM) image was performed on a Bruker Dimension Icon. The crystal structures of the samples were characterized using powder X-ray diffraction (Rigaku SmartLab (9 KW) diffractometer (Cu K $\alpha$  radiation) at settings of 45 kV and 200 mA). Raman spectra were recorded on DXR2xi Raman imaging microscopy under an excitation of 532 nm laser light. X-ray photoelectron spectroscopy (XPS) signals were obtained on a Thermo Escalab 250xi system with an Al K $\alpha$  X-ray monochromator (1486.6 eV). The Ni K-edge XAFS was measured at Singapore Synchrotron

Light Source. The light source provides a wide energy range of 1.2 - 12.8 keV with the resolving of  $\sim 3.8 \times 10^{-4}$  at 8 KeV. The NEXAFS measurement was performed in a vacuum at room temperature. The powder sample was compressed into tablet for test. Ni metal foil was used to calibrate the beam line energy. Thermogravimetric analysis was conducted on a TA Instruments METTLER TOLEDO in nitrogen atmosphere over a temperature range between 25 °C and 800 °C at a ramping rate 10 °C min<sup>-1</sup>. The specific surface area (Brunauer–Emmett–Teller (BET) method) was measured on an AutosorbiQ instrument (Quantachrome U.S.) with nitrogen adsorption-desorption isotherms at 77K. Electrochemical impedance spectroscopy (EIS) analysis was performed on Autolab PGSTAT 302 (Metrohm, Switzerland). The H<sub>2</sub> concentration was analyzed by gas chromatograph (Beijing Ruili) and the flow rate of carrier gas (Argon) was 32 sccm.

#### ***Preparation of working electrode.***

Electrocatalyst inks were prepared by mixing catalyst, dispersant and Nafion 117 solution. Specifically, catalyst (2 mg) was dispersed in 200 μL dispersant ( $V_{water} : V_{isopropanol} = 1:3$ ) first, then Nafion 117 solution (20 μL, 0.5 %) was added and the mixture was sonicated over 1.5 h until the catalyst was evenly dispersed. Finally, catalyst ink (50 μL) was painted directly onto the clean carbon paper ( $\sim 1 \text{ cm} \times 1.2 \text{ cm}$ ) and dried overnight at room temperature. After electrolysis, the electrode was rinsed with water thoroughly, dried in the air and used for morphology and surface chemical stage analysis through SEM, XRD and XPS to judge the stability of the material.

#### ***Electrocatalytic urea oxidation.***

Electrochemical tests were carried out in a three-electrode system on a workstation (CHI 600E Shanghai Chenhua Instrument Co. Ltd.). Catalyst loading carbon paper was used as working electrode and Hg / HgO electrode was used as reference electrode. Pt plate was selected as the counter electrode since Pt has almost no catalytic activity on UOR at the experimental potential and the effect of Pt dissolution on the catalytic effect can be ignored.<sup>1</sup> The reversible hydrogen electrode (RHE) potentials were obtained by the following equation:  $E(\text{RHE}) = E(\text{Hg} / \text{HgO}) + 0.059 \times \text{pH} + 0.098$ .

Before electrocatalytic urea oxidation experiment, the working electrode was activated by cyclic voltammetry (CV) in 1 M KOH solution until the signal was stable. The linear

sweep voltammetry (LSV) curve was recorded in the electrolyte of 1 M KOH + 0.33 M urea at a scan rate of 5 mV s<sup>-1</sup>. Electrochemically active surface area was determined by measuring the capacitive current associated with double-layer charging. The electric double layer capacitor ( $C_{dl}$ ) of the sample was obtained from CV plots in a non-Faraday range of 0.975~1.075 V (vs. RHE) with the scanning rates of 20, 40, 60, 80, and 100 mV s<sup>-1</sup> in 1 M KOH, and estimated by plotting the current density (mA cm<sup>-2</sup>) at 1.025 V (vs. RHE) against the scan rate (mV s<sup>-1</sup>). Electrochemical impedance spectroscopy (EIS) was measured at initial potential of 1.32 V (vs. RHE) from 0.1 Hz to 100 kHz with an amplitude of 5 mV in the electrolyte of 1 M KOH + 0.33 M urea. Chronoamperometric analysis was proceeded at the potential of 1.37 V (vs. RHE) and long-term CV cycling was carried out at the scan rate of 50 mV s<sup>-1</sup> in the electrolyte of 1 M KOH + 0.33 M urea. During the long-term i-t test, 10 mL of electrolyte was taken out every three hours for ICP-MS analysis in order to detect the concentration of Sn element in the electrolyte.

The test of the relationship between temperature and catalytic performance was carried out in a variable temperature water bath. If the reaction of electrocatalytic urea oxidation is accelerated during the increase of electrolyte temperature, the temperature dependence of the chemical rate constant is doubtless reflected. As showed in Equation S1, the Arrhenius relationship determines the apparent electrochemical activation energy ( $E_a$ ) of urea oxidation.<sup>2,3</sup>

$$\frac{\partial(\log i_k)}{\partial(1/T)} \Big|_{\eta} = \frac{E_a}{2.3R} \quad \text{S1}$$

where  $i_k$  (mA) is the kinetic current of materials. In this experiment, we chose the corresponding current density measured at the potential of 1.5 V (vs. RHE) in the electrolyte of 1 M KOH + 0.33 M urea at the scan rate of 20 mV s<sup>-1</sup>.  $T$  (K) represents the temperature of electrolyte, and  $R$  represents the universal gas constant. The apparent electrochemical activation energy can be extracted from the slop of the Arrhenius plots.

The concentration of H<sub>2</sub> was calculated by Equation S2:

$$C_{H_2} = \frac{V_{Ar} \times x_{\%}}{1000 \times m_{cats}} \quad \text{S2}$$

where  $C_{H_2}$  is the concentration of  $H_2$  ( $L \text{ min}^{-1} \text{ g}^{-1}_{\text{cat}}$ ).  $V_{Ar}$  is the flow rate of  $Ar$  (sccm).  $x\%$  is the volume fraction of hydrogen, which is calculated by the ratio of actual peak area to standard gas peak area.  $m_{\text{cats}}$  represents the loading amount of catalyst (g).

In the specific test process, the loading amount of P-NTS-0.5 catalyst was 0.5 mg and the flow rate of  $Ar$  was 32 sccm. In order to ensure the balance of gas concentration, the hydrogen concentration was tested after electrolysis for 15 min at each potential. The standard gas containing 0.2%  $H_2$  was used. Substituting all data into the above formula can obtain the volume of  $H_2$  produced by the unit mass catalyst per unit time at different potential. The test conditions of the two-electrode system were similar to the three-electrode system, with dry batteries as the power source, carbon paper loaded with 0.5 mg P-NTS-0.5 as the working electrode, and platinum sheet electrode as the counter electrode. Due to the low hydrogen production at low potential, the flow rate of the argon was set to 20 sccm.

### ***Calculations.***

When carrying out DFT calculation, Perdew-Burke-Ernzerhof (PBE) exchange-correlation functional was used with a plane wave pseudopotential implementation.<sup>4</sup> The kinetic energy cutoff was set to 380 eV. The (220) facet of cubic  $NiS_2$  was selected as the model. The model was a periodic unit cell ( $3 \times 3 \times 2$ ), and Gamma k-point was adopted. One Ni (II) atom on the surface was substituted by a Sn (IV) atom to generate S vacancy. The surface atoms were completely relaxed to obtain accurate adsorptive configuration.

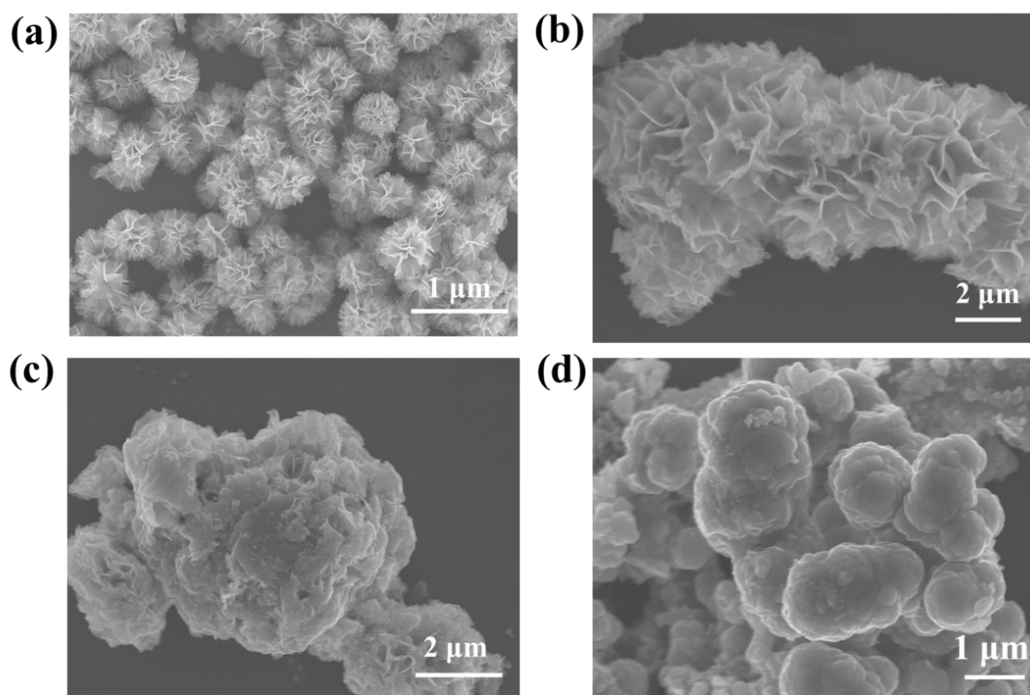


**Figure S1.** SEM images of (a) SnS<sub>2</sub>, (b) F-TNS-0.3, (c) F-TNS-0.7, and (d) control group NS.

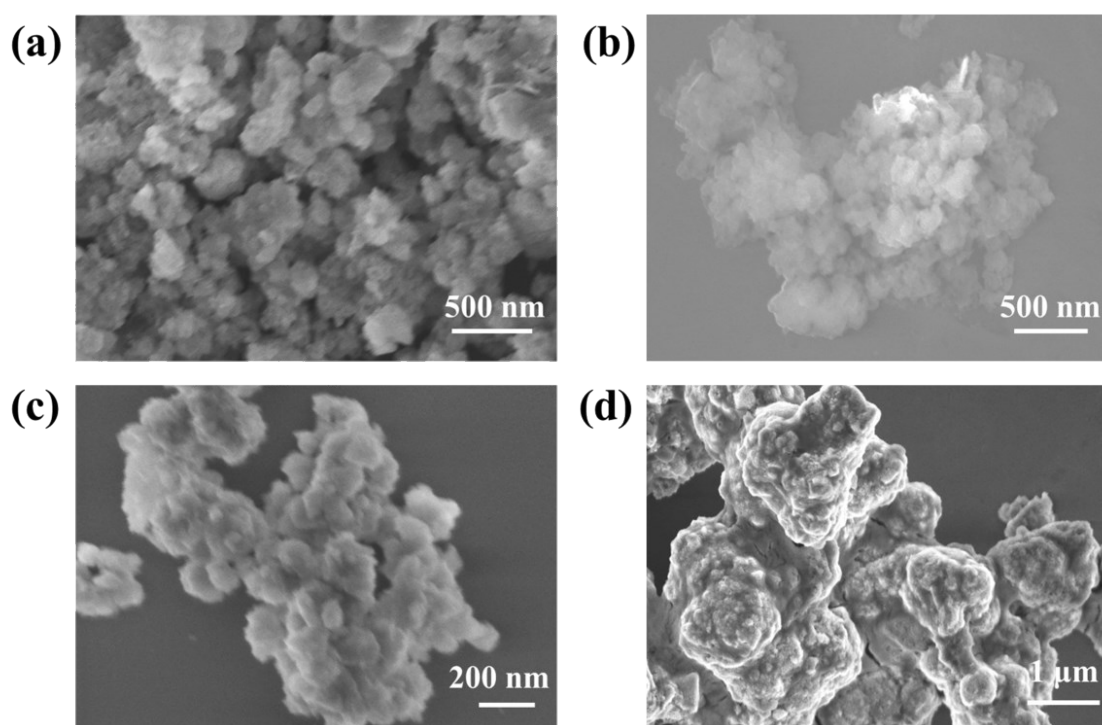


**Figure S2.** SEM images of (a) P-NTS-0.3, (b) P-NTS-0.5, (c) P-NTS-0.7, and (d) control group NS-KOH.

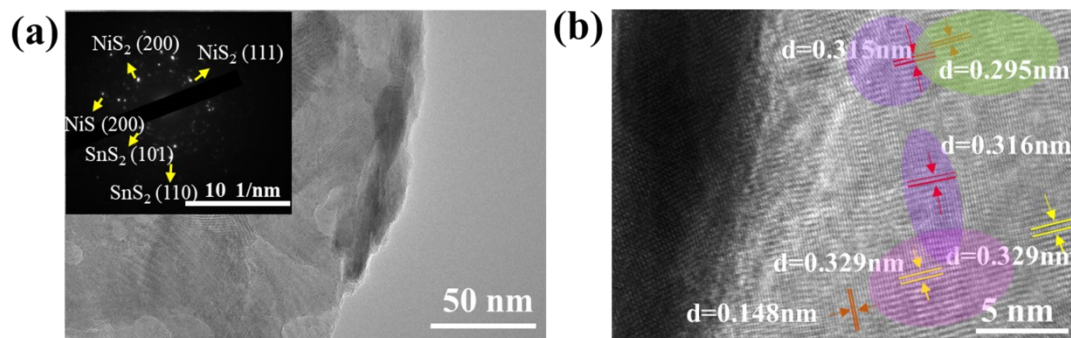


**Figure S3.** (a and inset) HRTEM image and SAED pattern of the F-TNS-0.5, (b) Partial enlarged HRTEM of F-TNS-0.5. The purple area represents SnS<sub>2</sub>, the magenta area represents NiS<sub>2</sub>, and the green area represents NiS.

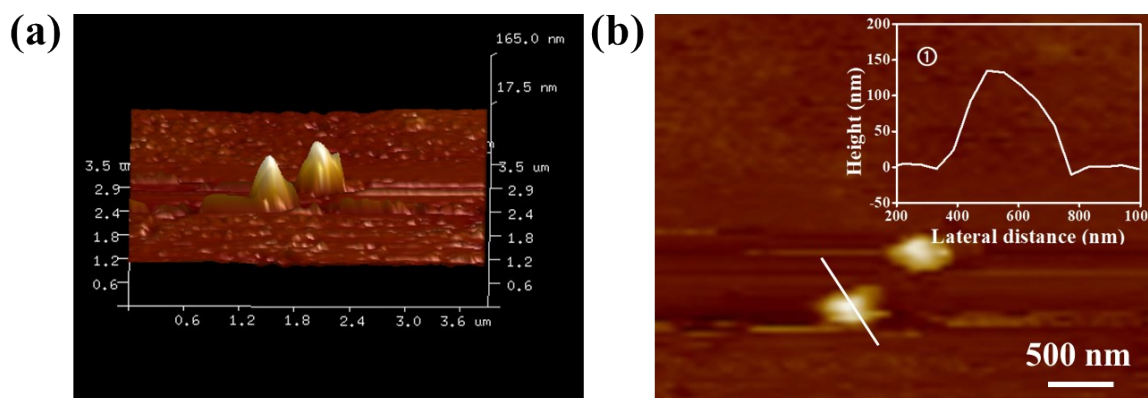


**Figure S4.** (a) AFM image and (b) height profile of P-NTS-0.5.

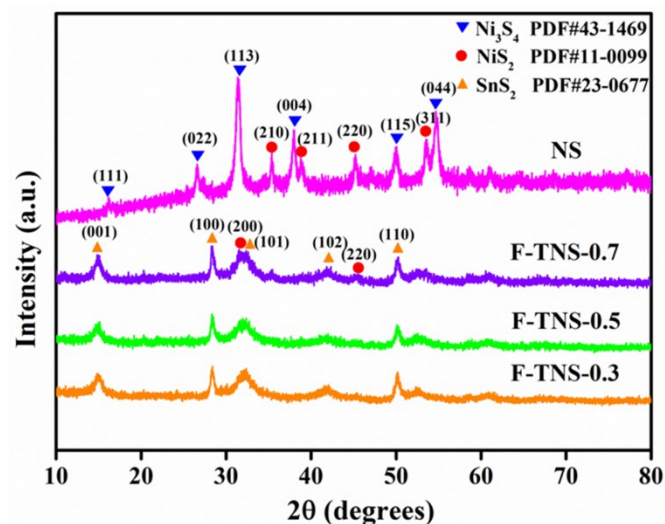


**Figure S5.** Powder XRD patterns of F-TNS and control group NS.

As shown in control group NS sample,  $\text{Ni}_3\text{S}_4$  and  $\text{NiS}_2$  were main ingredients. In F-TNS-0.3, F-TNS-0.5 and F-TNS-0.7 samples, most of the diffraction peaks belong to  $\text{SnS}_2$ , but  $\text{NiS}_2$  (200) and  $\text{NiS}_2$  (220) crystal planes gradually appeared with the increase of Ni content.

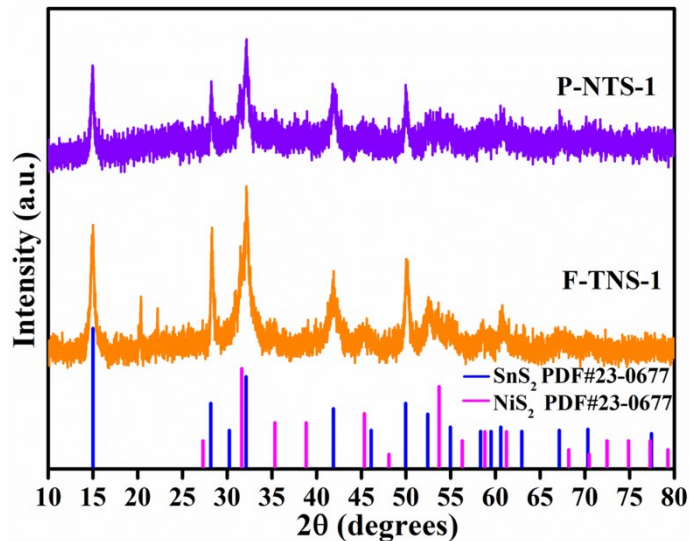


**Figure S6.** Powder XRD patterns of F-TNS-1 and P-NTS-1.

When the molar ratio of Sn to Ni was 1:1,  $\text{SnS}_2$  and  $\text{NiS}_2$  coexisted in F-TNS-1. However, after 1 M KOH etching, the diffraction peaks of  $\text{SnS}_2$  still exist in P-NTS-1 obviously, which were quite different from P-NTS-0.3 and P-NTS-0.5.

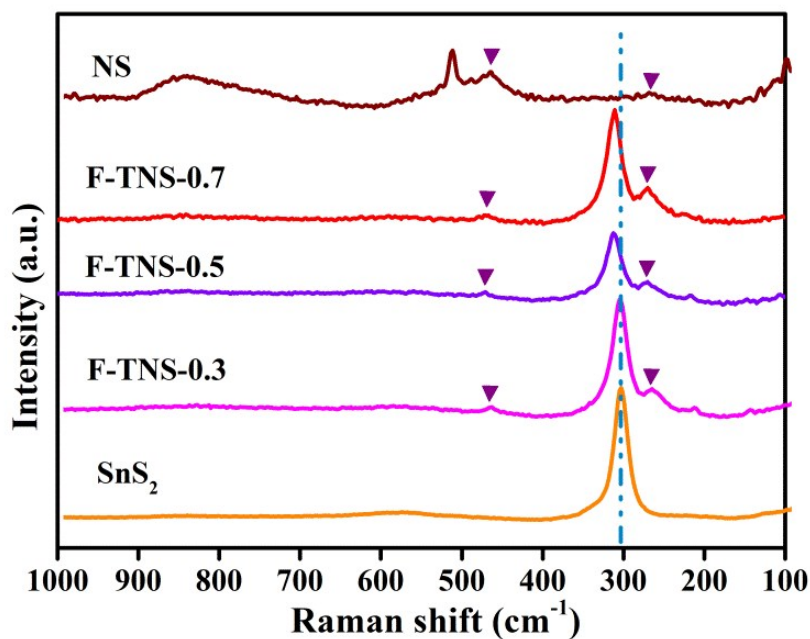


**Figure S7.** Raman spectra of SnS<sub>2</sub>, F-TNS and control group NS.

For pure SnS<sub>2</sub>, the peak located at around 314 cm<sup>-1</sup> corresponds to the A<sub>1g</sub> mode of SnS<sub>2</sub>.<sup>5</sup> However, the peak of SnS<sub>2</sub> positively shifted in all F-TNS samples, indicating the introduction of Ni<sup>2+</sup> contributes to the degree of disorder, and the strong interactions between Sn and Ni exist in F-TNS. The peaks located at 278.8 cm<sup>-1</sup> and 478.4 cm<sup>-1</sup> correspond to the E<sub>g</sub> and A<sub>g</sub> phonon models of the NiS<sub>2</sub> Raman feature, respectively.<sup>6,7</sup> The introduction of Sn element into the lattice of NiS<sub>2</sub> and the interface effect between NiS<sub>2</sub> and SnS<sub>2</sub> made the E<sub>g</sub> and A<sub>g</sub> phonon models of NiS<sub>2</sub> shifted positively.

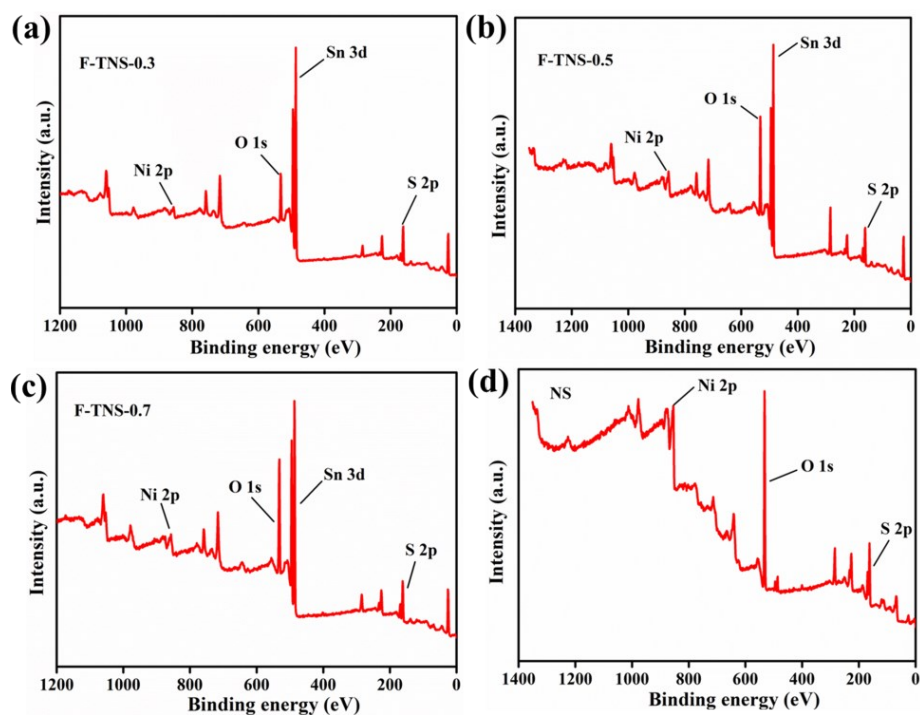


**Figure S8.** (a-d) Full XPS spectra of F-TNS and control group NS.

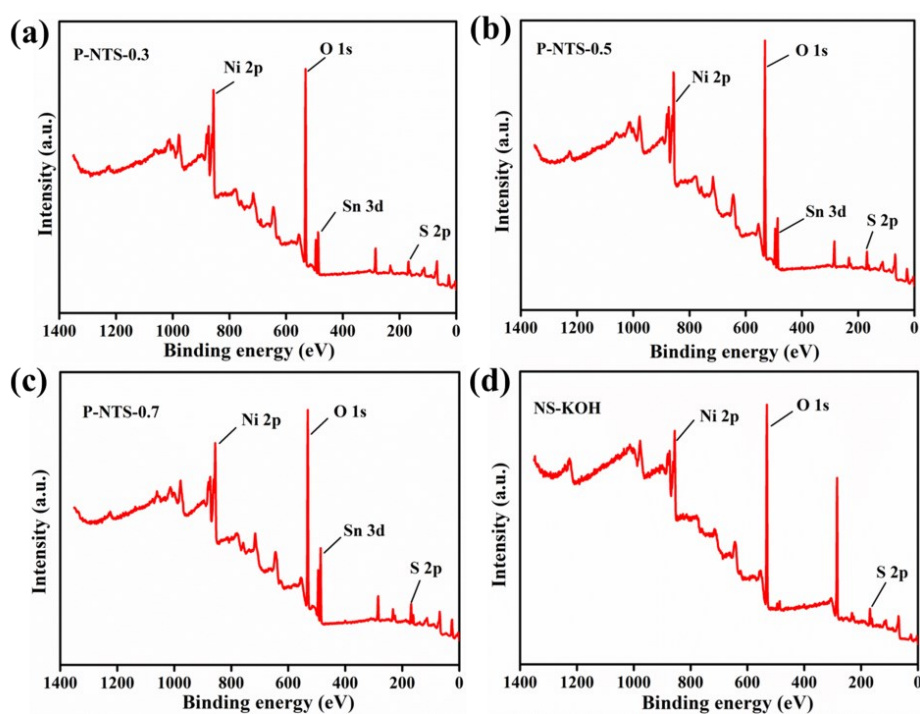


**Figure S9.** (a-d) Full XPS spectra of P-NTS and control group NS-KOH.

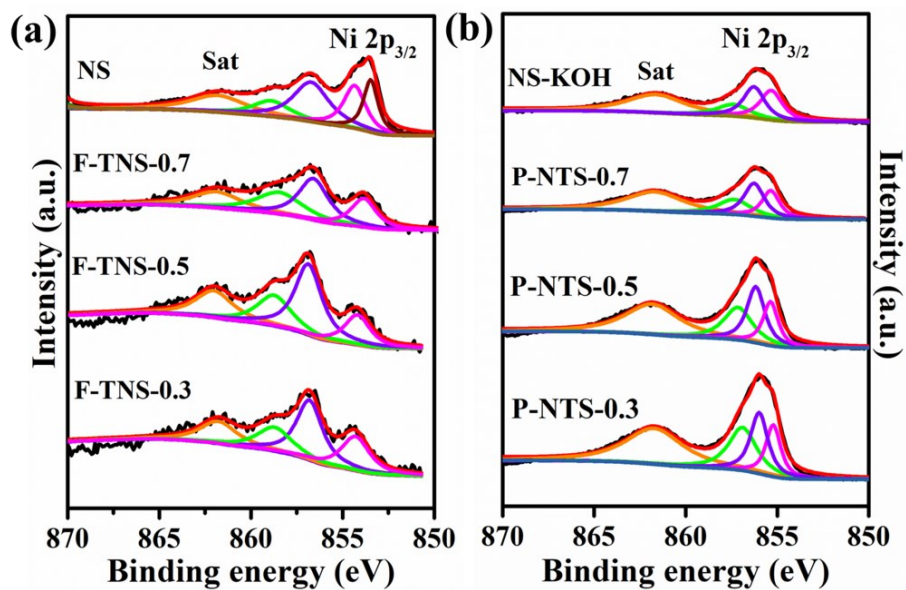


**Figure S10.** XPS Ni 2p<sub>3/2</sub> spectra of (a) F-TNS and control group NS, and (b) P-NTS and control group NS-KOH.

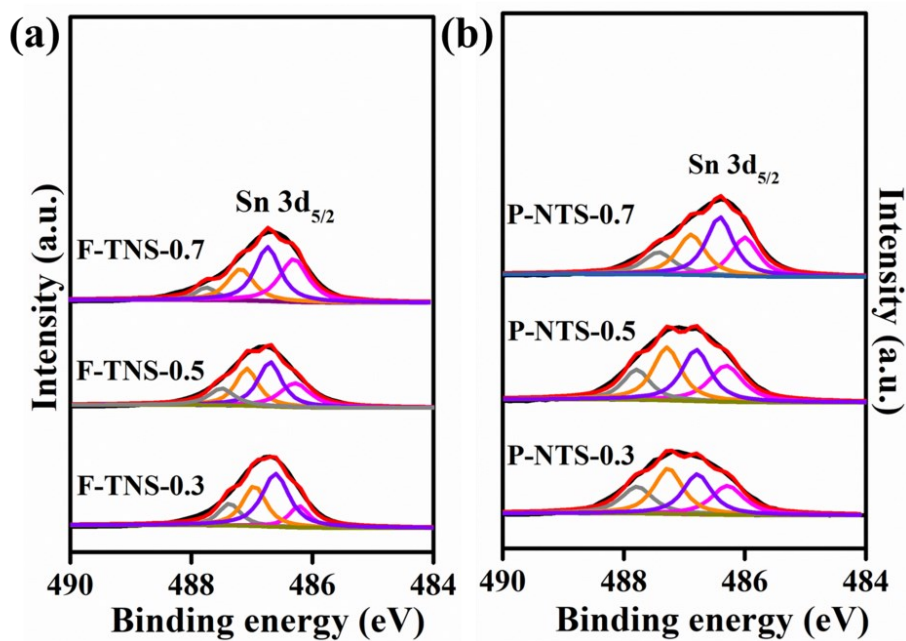


**Figure S11.** XPS Sn 3d<sub>5/2</sub> spectra of (a) F-TNS and (b) P-NTS.

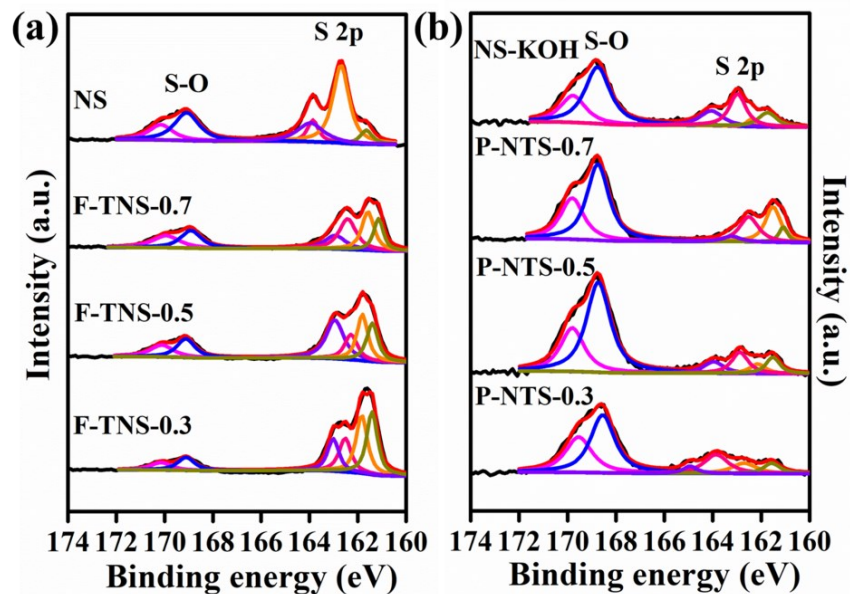


**Figure S12.** XPS S 2p spectra of (a) F-TNS and control group NS, and (b) P-NTS and control group NS-KOH.

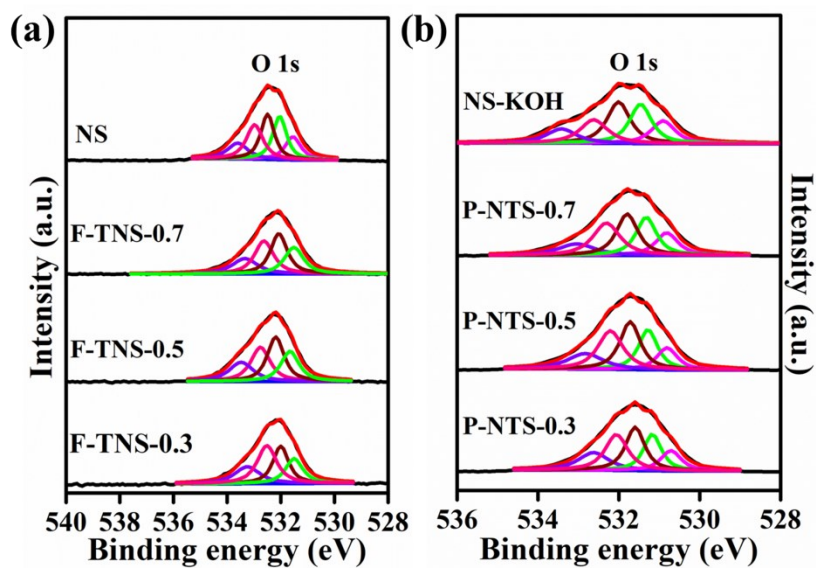


**Figure S13.** XPS O 1s spectra of (a) F-TNS and control group NS, and (b) P-NTS and control group NS-KOH.

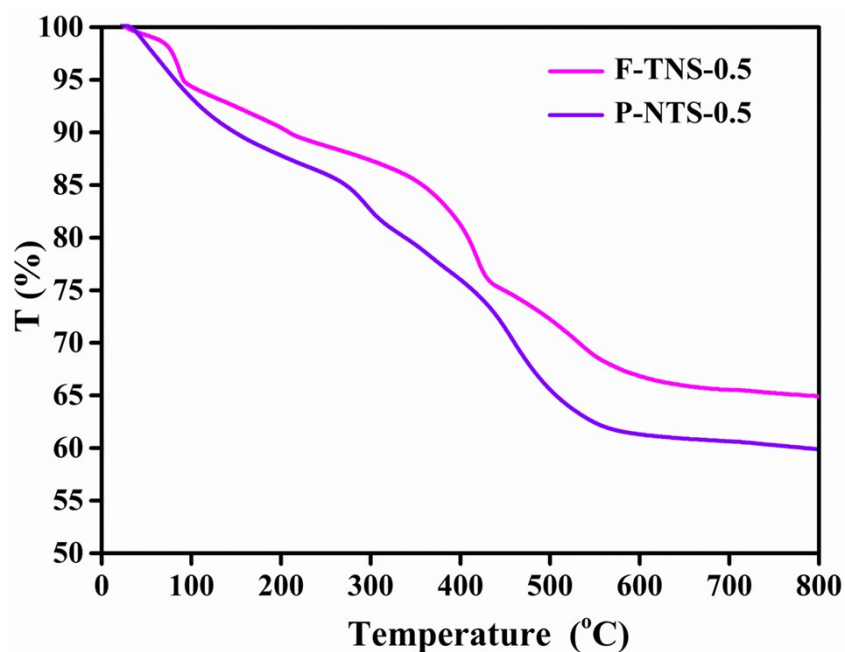


**Figure S14.** TGA results of F-TNS-0.5 and P-NTS-0.5 recorded from 25 °C to 800 °C at a ramping rate of 10 °C min<sup>-1</sup>.

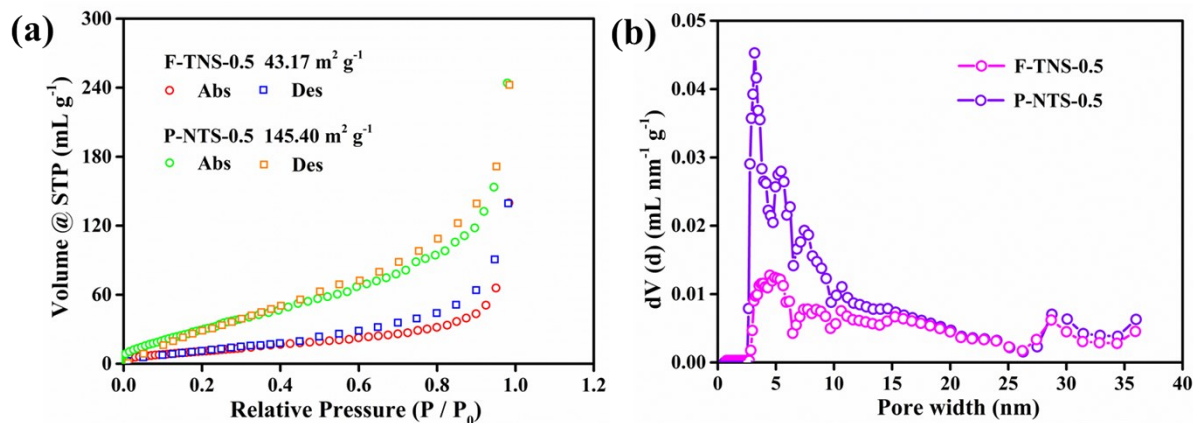


**Figure S15.** (a) Nitrogen adsorption-desorption isotherms for F-TNS-0.5 and P-NTS-0.5. (b) Corresponding pore size distribution curve of F-TNS-0.5 and P-NTS-0.5.

The specific surface areas of F-TNS-0.5 and P-NTS-0.5 were 43.17 m<sup>2</sup> g<sup>-1</sup> and 145.40 m<sup>2</sup> g<sup>-1</sup>, respectively. The pore size distribution obtained by the BJH model showed that P-NTS-0.5 sample was more mesoporous and the size was around 3 nm.

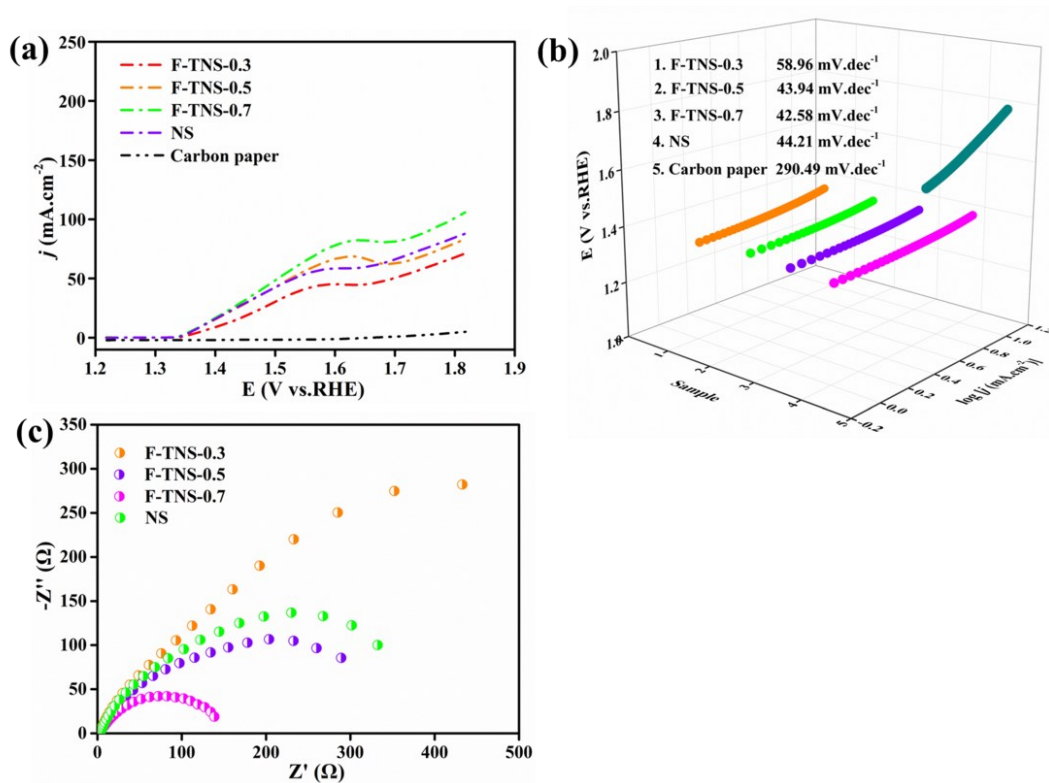


**Figure S16.** (a) Linear sweep voltammetry (LSV) curves of F-TNS, control group NS and carbon paper in the electrolyte of 1.0 M KOH + 0.33 M urea at the scan rate of 5 mV s<sup>-1</sup>, (b) Tafel plots of F-TNS, control group NS and carbon paper, and (c) Nyquist plots of F-TNS and control group NS.

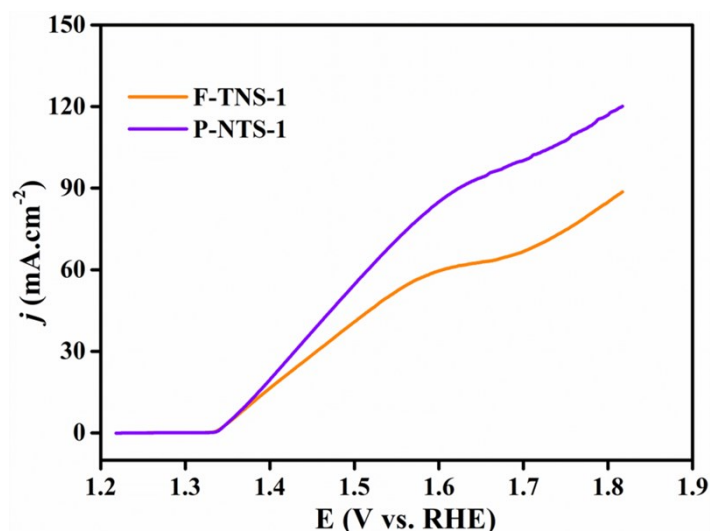


**Figure S17.** LSV curves of F-TNS-1 and P-NTS-1 measured in the electrolyte of 1.0 M KOH + 0.33M urea at the scan rate of 5 mV s<sup>-1</sup>.

The UOR performance of P-NTS-1 was lower than that of P-NTS-0.7, although it was higher than F-TNS-1. Combining with the XRD results of P-NTS, we can draw the conclusion that the presence of SnS<sub>2</sub> in the materials can restrain UOR activity, and only doping Sn atom into the lattice of NiS<sub>2</sub> with the optimal amount of Ni-Sn dual active sites can boost UOR ultimately.

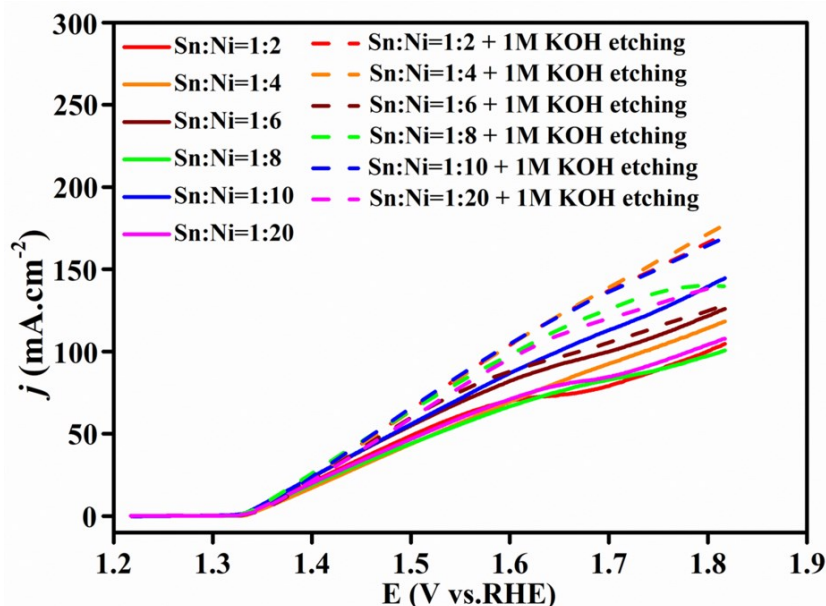


**Figure S18.** LSV curves of a series of Ni-Sn sulfides with and without the step of 1 M KOH etching. The ratios marked in the figure represented the molar ratio of SnCl<sub>4</sub> and NiCl<sub>2</sub>•6H<sub>2</sub>O when making SnNiS precursor.

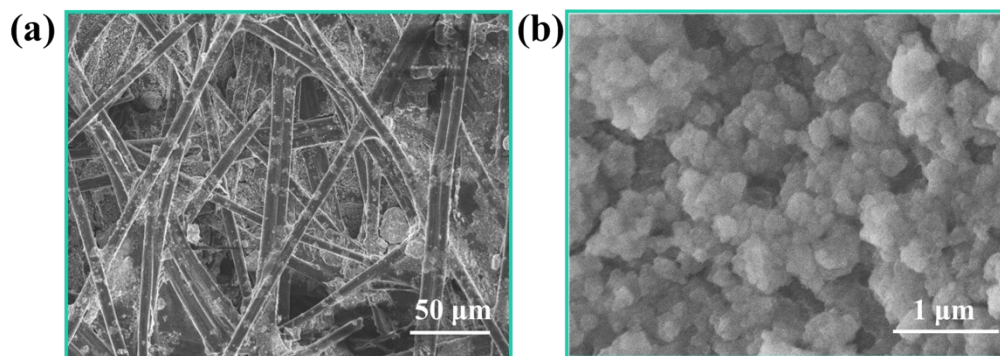


**Figure S19.** (a) SEM image and (b) partially enlarged SEM image of P-NTS-0.5 dripping on carbon paper after UOR test.

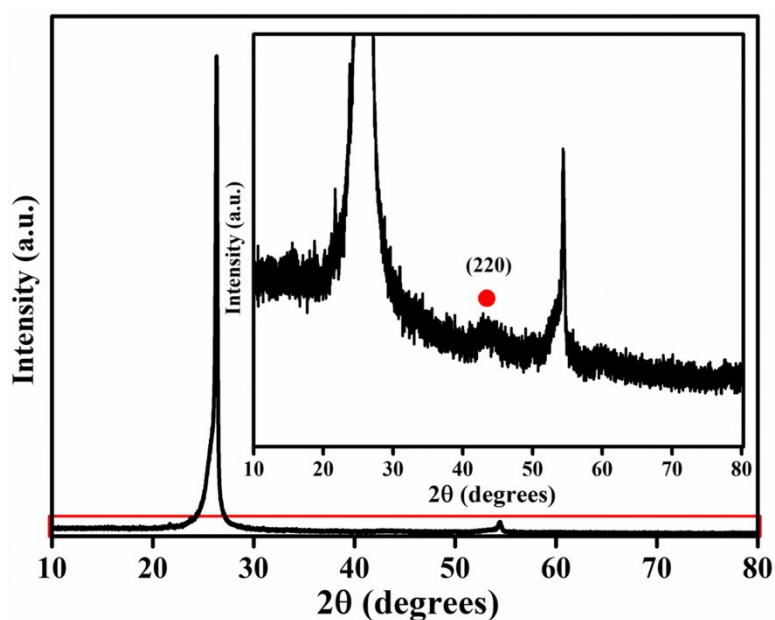


**Figure S20.** Powder XRD patterns of P-NTS-0.5 dripping on carbon paper after UOR test.

The peak located at 26.35° and 54.38° were ascribed to carbon. The peak ascribing to NiS<sub>2</sub> (220) still existed in P-NTS-0.5, indicating the good stability of this sample.

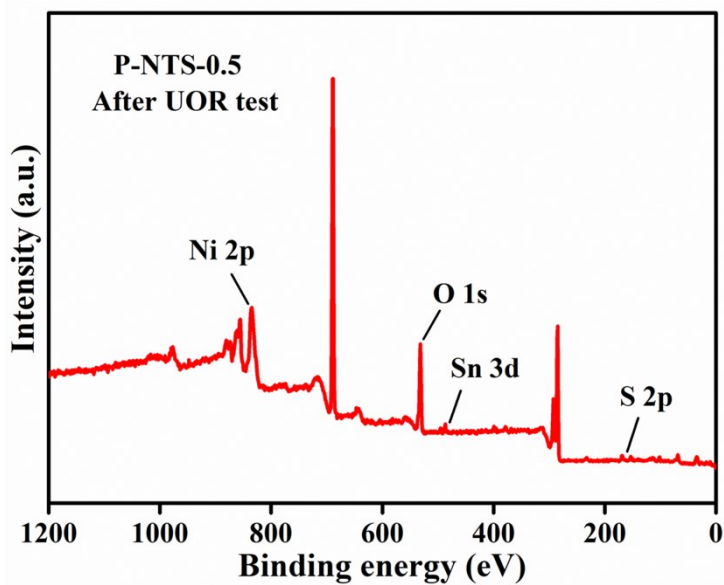


**Figure 21.** Full XPS spectrum of P-NTS-0.5 dripping on carbon paper after UOR test.

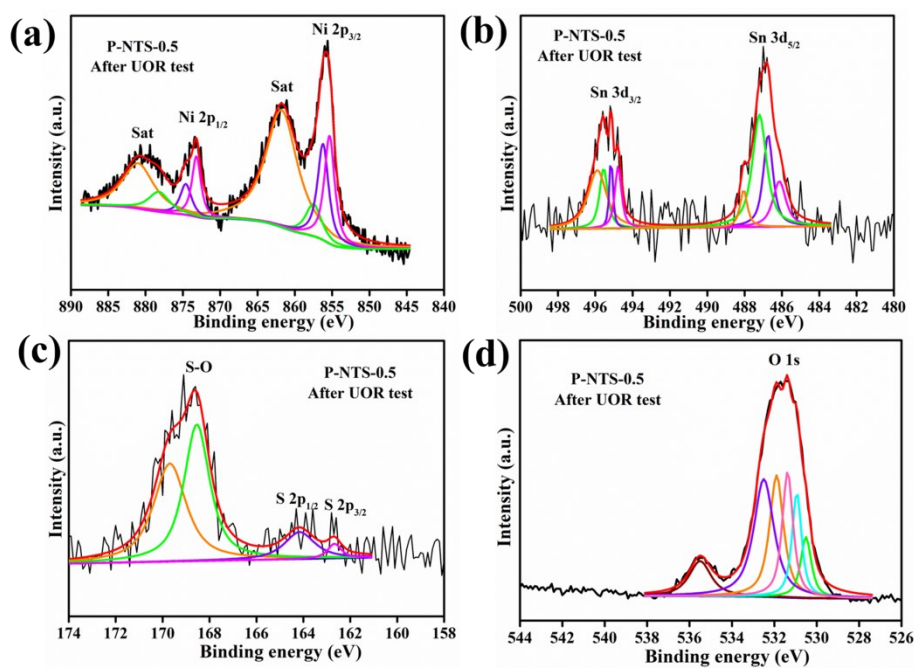


**Figure S22.** XPS spectra of (a) Ni 2p, (b) Sn 3d, (c) S 2p, and (d) O 1s for P-NTS-0.5 dripping on carbon paper after UOR test.

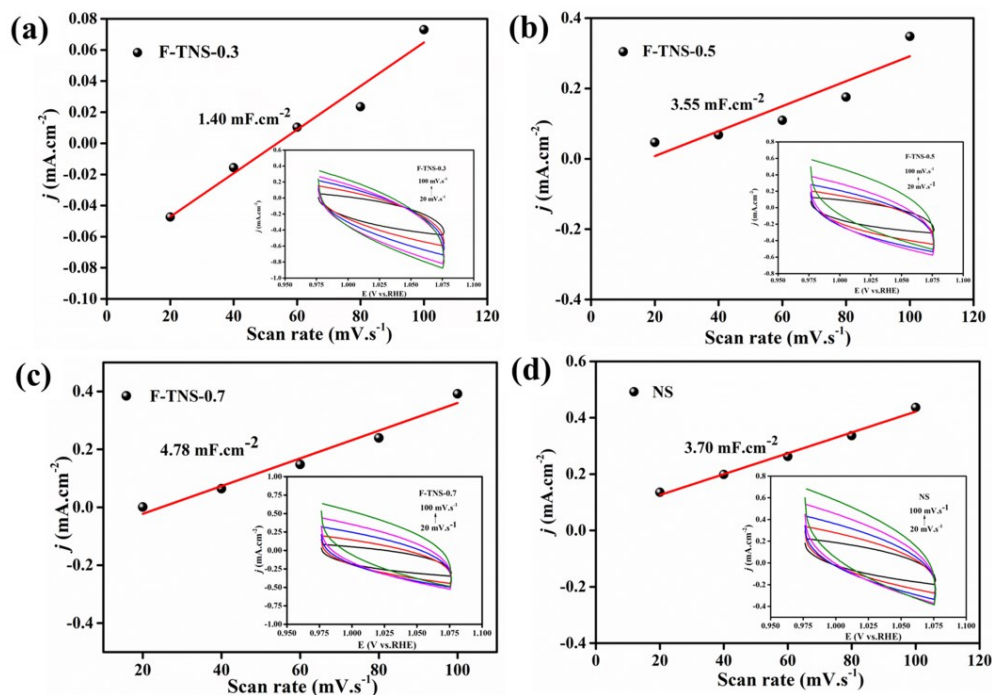


**Figure S23.** Scan rate-dependent current densities to estimate the  $C_{dl}$  of (a) F-TNS-0.3, (b) F-TNS-0.5, (c) F-TNS-0.7, and (d) control group NS. The insets were the CV cycles measured at the scan rates of 20, 40, 60, 80, and 100  $\text{mV s}^{-1}$  in the potential region of 0.975–1.075 V (vs. RHE), respectively.

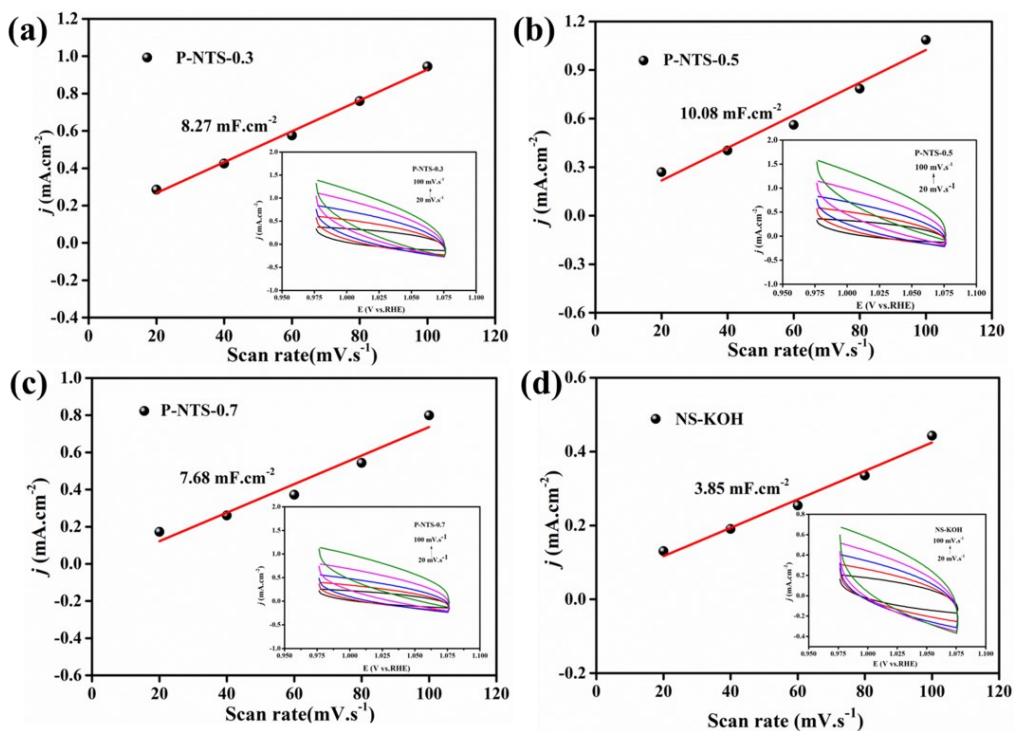


**Figure S24.** Scan rate-dependent current densities to estimate the  $C_{dl}$  of (a) P-NTS-0.3, (b) P-NTS-0.5, (c) P-NTS-0.7, and (d) control group NS-KOH. The insets were the CV cycles

measured at the scan rate of 20, 40, 60, 80, and 100  $\text{mV s}^{-1}$  in the potential region of 0.975-1.075 V (vs. RHE), respectively.

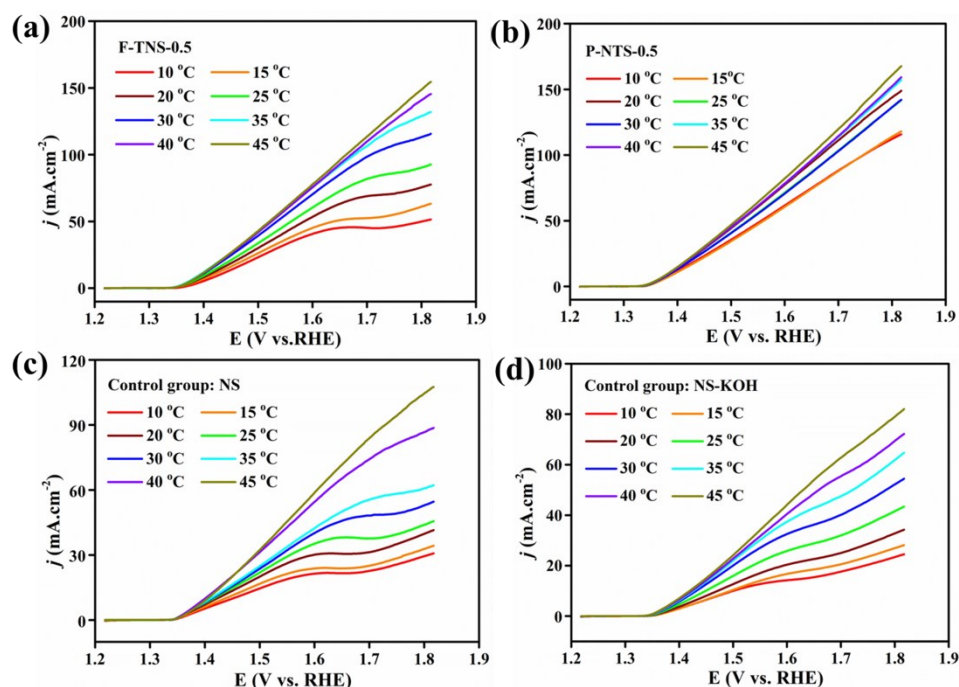


**Figure S25.** LSV curves of (a) F-TNS-0.5, (b) P-NTS-0.5, (c) control group NS, and (d) NS-KOH in the electrolyte of 1 M KOH + 0.33 M urea at the temperature of 10 °C, 15 °C, 20 °C, 25 °C, 30 °C, 35 °C, 40 °C, and 45 °C, respectively.

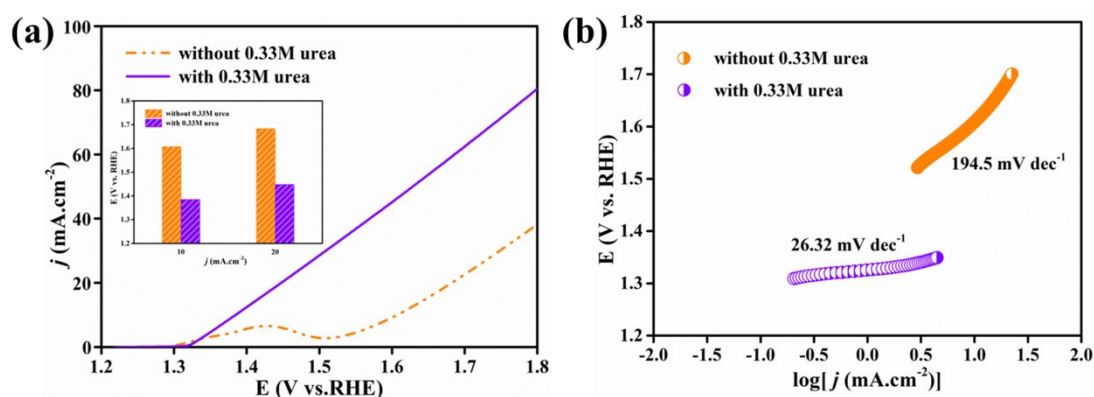


**Figure S26.** (a and inset) LSV curves and potential comparison for achieving current densities of 10 and 20  $\text{mA}\cdot\text{cm}^{-2}$  over P-NTS-0.5 / P-NTS-0.5 in 1.0 M KOH electrolyte and 1.0 M KOH + 0.33 M urea electrolyte, respectively. (b) Corresponding Tafel slopes of OER (1 M KOH) and UOR (1 M KOH + 0.33 M urea).

**Table S1.** Ni 2p<sub>3/2</sub> XPS analysis results of F-TNS, P-NTS and control groups NS and NS-KOH.

Sample	Satellite peak	Ni-O	Ni-S	Ni-S	Ni-S
F-TNS-0.3	861.77	858.71	856.80	854.28	
F-TNS-0.5	862.03	858.74	856.87	854.18	
F-TNS-0.7	861.93	858.56	856.72	854.00	
NS	861.60	858.96	856.73	854.28	853.45
Sample	Satellite peak	Ni-O	Ni-OH, Ni-S	Ni-S	
P-NTS-0.3	861.72	856.89	855.99	855.22	
P-NTS-0.5	861.82	857.15	856.18	855.38	
P-NTS-0.7	861.72	857.34	856.32	855.40	
NS-KOH	861.65	857.43	856.30	855.36	

**Table S2.** Sn 3d<sub>5/2</sub> XPS analysis results of F-TNS and P-NTS.

Sample	Sn <sup>4+</sup> -O	Sn <sup>4+</sup> -S	Sn <sup>2+</sup> -O	Sn <sup>2+</sup> -S
F-TNS-0.3	487.37	486.95	486.60	486.22
F-TNS-0.5	487.52	487.10	486.72	486.31
F-TNS-0.7	487.72	487.15	486.70	486.27
Sample	SnO <sub>3</sub> <sup>2-</sup>	Sn <sup>4+</sup> -S	Sn <sup>2+</sup> -O	Sn <sup>2+</sup> -S
P-NTS-0.3	487.78	487.27	486.79	486.29
P-NTS-0.5	487.80	487.30	486.81	486.32
P-NTS-0.7	487.53	486.99	486.52	486.10

**Table S3.** S 2p XPS analysis results of F-TNS, P-NTS and control groups NS and NS-KOH.

<b>Sample</b>	<b>S<sup>6+</sup>-O</b>	<b>S<sup>4+</sup>-O</b>	<b>2p<sub>1/2</sub> S-Metal</b>		<b>2p<sub>3/2</sub> S-Metal</b>	
F-TNS-0.3	170.15	169.10	162.90	162.40	161.90	161.40
F-TNS-0.5	170.13	169.13	162.95	162.29	161.81	161.40
F-TNS-0.7	170.00	169.37	163.00	162.48	161.48	161.20
NS	170.13	169.13	162.95	162.29	161.81	161.40
<b>Sample</b>	<b>S<sup>6+</sup>-O</b>	<b>S<sup>4+</sup>-O</b>	<b>2p<sub>1/2</sub> S-Metal</b>		<b>2p<sub>3/2</sub> S-Metal</b>	
P-NTS-0.3	172.08	168.55	164.92	163.86	162.71	161.56
P-NTS-0.5	169.83	168.75	163.99	162.90	162.16	161.54
P-NTS-0.7	169.83	168.77	163.27	162.56	161.57	161.14
NS-KOH	169.83	168.82	164.12	163.03	162.46	161.79

**Table S4.** O 1s XPS analysis results of F-TNS, P-NTS and control groups NS and NS-KOH.

<b>Sample</b>	<b>O<sub>2</sub></b>	<b>-OH</b>	<b>O-S</b>	<b>O-Metal</b>	
F-TNS-0.3	533.20	532.50	531.99	531.50	
F-TNS-0.5	533.50	532.78	532.21	531.68	
F-TNS-0.7	533.32	532.61	532.06	531.49	
NS	533.61	532.98	532.50	532.04	531.55
<b>Sample</b>	<b>-OH</b>	<b>O-S</b>	<b>O-Metal</b>		
P-NTS-0.3	532.62	532.06	531.60	531.17	530.71
P-NTS-0.5	532.80	532.19	531.70	531.26	530.79
P-NTS-0.7	533.06	532.32	531.81	531.34	530.84
NS-KOH	533.41	532.61	531.99	531.45	530.89

**Table S5.** Electrochemical parameters of the investigated materials when driving the UOR process as anode in the electrolyte of 1 M KOH + 0.33M urea ( $E = 10 \text{ mA cm}^{-2}$ ,  $j = 1.5 \text{ V}$  (vs. RHE) without  $iR$ -compensation).

Parameters	F-TNS-0.3	F-TNS-0.5	F-TNS-0.7	NS	P-NTS-0.3	P-NTS-0.5	P-NTS-0.7	NS-KOH
<b>E</b> (V vs. RHE)	1.41	1.38	1.38	1.38	1.38	1.36	1.37	1.37
<b>j</b> ( $\text{mA cm}^{-2}$ )	30.5	42.7	48.7	42.6	67.2	76.4	68.7	46.2
<b>Tafel slope</b> ( $\text{mV dec}^{-1}$ )	58.96	43.94	42.58	44.21	33.52	32.30	36.45	45.68
<b><math>C_{dl}</math></b> ( $\text{mF cm}^{-2}$ )	1.40	3.55	4.78	3.70	8.27	10.08	7.68	3.85
<b><math>R_s</math></b> (ohm)	1.47	1.68	1.64	1.68	1.49	1.45	1.55	1.58
<b><math>R_p</math></b> (ohm)	908.6	374.6	165.0	464.8	55.5	51.8	67.0	235.7

**Table S6.** Concentration of Sn element in the electrolyte after  $i$ - $t$  test of 0 h, 3 h, 6 h, 9 h and 12 h.

Time / h	0	3	6	9	12
<b>Sn content / <math>\text{ng mL}^{-1}</math></b>	0.82	6.12	15.05	15.67	15.42

**Table S7.** Hydrogen generation rate at different potentials in a two-electrode system.

Potential / V (vs. RHE)	1.5	2.3	3.1
<b><math>\text{H}_2 / \text{L min}^{-1} \text{g}^{-1}_{\text{cat}}</math></b>	1.6	94.8	200.4

**Table S8.** Electrocatalytic performance of urea oxidation compared with previously reported work.

Catalyst	E @ 10 mA cm <sup>-2</sup> (V vs. RHE)	j @ 1.5V (vs. RHE) (mA cm <sup>-2</sup> )	Substrate	Electrolyte KOH / urea (M / M)	References
<b>P-NTS-0.5</b>	<b>1.36</b>	<b>76</b>	<b>CC</b>	<b>1 / 0.33</b>	<b>This work</b>
<b>S-Ni(OH)<sub>2</sub></b>	1.39	32	GC	1 / 0.33	8
<b>Ni-MOF</b>	1.36	75	GC	1 / 0.33	9
<b>Ni/C</b>	1.38	26	GC	1 / 0.33	10
<b>Ni<sub>3</sub>S<sub>2</sub> nanowires</b>	1.36	10	NF	1 (NaOH) / 0.2	11
<b>Ni@GO</b>	1.45	15	GC	1 / 0.33	12
<b>NiO</b>	1.39	48	NF	1 / 0.33	13
<b>V<sub>Ni</sub>-<math>\alpha</math>-Ni(OH)<sub>2</sub>-4</b>	1.39	70	GC	1 / 0.33	14
<b>Ni(OH)<sub>2</sub></b>	1.45	45	GC	1 / 0.33	15
<b>NiOH-D</b>	1.35	50	GC	1 / 0.33	16
<b>Ni(OH)<sub>2</sub></b>	1.38	60	GC	1 / 0.33	17
<b>ML Ni(OH)<sub>2</sub> NS</b>	1.58	9	CC	1 / 0.33	18
<b>NiCoO</b>	1.38	50	GC	1 / 0.33	19
<b>NiCo-LDH-NO<sub>3</sub></b>	1.32	50	RDE	1 / 0.33	20
<b>MOF-Ni@MOF-Fe</b>	1.35	125	NF	1/0.5	21
<b>CoNi-LDH</b>	1.38	160	NF	1 / 0.5	22
<b>Ni(OH)<sub>2</sub>/MnO<sub>2</sub></b>	1.46	13	CC	1 / 0.5	23
<b>CeO<sub>2</sub>-NiMoO<sub>4</sub></b>	1.35	130	NF	1 / 0.33	24

CC: Carbon cloth; NF: nickel foam; RDE: Rotating disk electrode; GC: glassy carbon electrode.

## References

- 1 B. K. Boggs, R. L. King and G. G. Botte, *Chem. Commun.*, 2009, 4859-4861.
- 2 X. Zheng, B. Zhang, P. De Luna, Y. Liang, R. Comin, O. Voznyy, L. Han, F. P. Garcia de Arquer, M. Liu, C. T. Dinh, T. Regier, J. J. Dynes, S. He, H. L. Xin, H. Peng, D. Prendergast, X. Du and E. H. Sargent, *Nat. Chem.*, 2018, **10**, 149-154.

- 3 W. Wang, Y. B. Zhu, Q. Wen, Y. Wang, J. Xia, C. Li, M. W. Chen, Y. Liu, H. Li, H. A. Wu and T. Zhai, *Adv. Mater.*, 2019, **31**, 1900528.
- 4 J. P. Perdew, K. Bruke and M. Ernzerhof, *Phy. Rev. Lett.*, 1996, **77**, 3865-3868.
- 5 B. Li, T. Xing, M. Zhong, L. Huang, N. Lei, J. Zhang, J. Li and Z. Wei, *Nat. Commun.*, 2017, **8**, 1958.
- 6 J. Wang, Z. Liu, C. Zhan, K. Zhang, X. Lai, J. Tu and Y. Cao, *J. Mater. Sci. Technol.*, 2020, **39**, 155-160.
- 7 D. Zhang, H. Mou, L. Chen, G. Xing, D. Wang and C. Song, *Nanoscale*, 2020, **12**, 3370-3376.
- 8 X. Zhu, X. Dou, J. Dai, X. An, Y. Guo, L. Zhang, S. Tao, J. Zhao, W. Chu, X. C. Zeng, C. Wu and Y. Xie, *Angew. Chem. Int. Ed.*, 2016, **55**, 12465-12469.
- 9 D. Zhu, C. Guo, J. Liu, L. Wang, Y. Du and S. Z. Qiao, *Chem. Commun.*, 2017, **53**, 10906-10909.
- 10 L. Wang, L. Ren, X. Wang, X. Feng, J. Zhou and B. Wang, *ACS Appl. Mater. Interfaces*, 2018, **10**, 4750-4756.
- 11 M. Liu, Y. Jiao, S. Zhan and H. Wang, *Catal. Today*, 2020, doi: 10.1016/j.cattod.2019.05.032.
- 12 A. V. Munde, B. B. Mulik, P. P. Chavan and B. R. Sathe, *Electrochimi. Acta*, 2020, doi: 10.1016/j.electacta.2020.136386.
- 13 M.-S. Wu, F.-Y. Chen, Y.-H. Lai and Y.-J. Sie, *Electrochimi. Acta*, 2017, **258**, 167-174.
- 14 Q. He, Y. Wan, H. Jiang, Z. Pan, C. Wu, M. Wang, X. Wu, B. Ye, P. M. Ajayan and L. Song, *ACS Energy Lett.*, 2018, **3**, 1373-1380.
- 15 W. Yang, X. Yang, B. Li, J. Lin, H. Gao, C. Hou and X. Luo, *J. Mater. Chem. A*, 2019, **7**, 26364-26370.
- 16 L. Zhang, L. Wang, H. Lin, Y. Liu, J. Ye, Y. Wen, A. Chen, L. Wang, F. Ni, Z. Zhou, S. Sun, Y. Li, B. Zhang and H. Peng, *Angew. Chem. Int. Ed.*, 2019, **58**, 16820-16825.
- 17 W. Yang, X. Yang, C. Hou, B. Li, H. Gao, J. Lin and X. Luo, *Appl. Cataly. B*, 2019, **259**, 118020.
- 18 C. Lin, Z. Gao, F. Zhang, J. Yang, B. Liu and J. Jin, *J. Mater. Chem. A*, 2018, **6**, 13867-13873.
- 19 S. Wang, X. Yang, Z. Liu, D. Yang and L. Feng, *Nanoscale*, 2020, **12**, 10827-10833.
- 20 M. Zeng, J. Wu, Z. Li, H. Wu, J. Wang, H. Wang, L. He and X. Yang, *ACS Sustainable Chem. Eng.*, 2019, **7**, 4777-4783.
- 21 H. Xu, K. Ye, K. Zhu, J. Yin, J. Yan, G. Wang and D. Cao, *Dalton Trans.*, 2020, **49**, 5646-5652.
- 22 Y. Feng, X. Wang, J. Huang, P. Dong, J. Ji, J. Li, L. Cao, L. Feng, P. Jin and C. Wang, *Chem. Eng.*

*J.*, 2020, **390**, 124525.

23 J. Meng, P. Chernev, M. R. Mohammadi, K. Klingan, S. Loos, C. Pasquini, P. Kubella, S. Jiang, X.

Yang, Z. Cui, S. Zhu, Z. Li, Y. Liang and H. Dau, *Electrochimi. Acta*, 2019, **318**, 32-41.

24 W. Gao, C. Wang, F. Ma and D. Wen, *Electrochimi. Acta*, 2019, **320**, 134608.